

Computing the rearrangement distance of natural genomes

Leonard Bohnenkämper, Marília D. V. Braga, Daniel Doerr, and Jens Stoye

Faculty of Technology and Center for Biotechnology (CeBiTec), Bielefeld University, Bielefeld, Germany

Abstract. The computation of genomic distances has been a very active field of computational comparative genomics over the last 25 years. Substantial results include the polynomial-time computability of the inversion distance by Hannenhalli and Pevzner in 1995 and the introduction of the double-cut and join (DCJ) distance by Yancopoulos, Attie and Friedberg in 2005. Both results, however, rely on the assumption that the genomes under comparison contain the same set of unique *markers* (syntenic genomic regions, sometimes also referred to as *genes*). In 2015, Shao, Lin and Moret relax this condition by allowing for duplicate markers in the analysis. This generalized version of the genomic distance problem is NP-hard, and they give an ILP solution that is efficient enough to be applied to real-world datasets. A restriction of their approach is that it can be applied only to *balanced* genomes, that have equal numbers of duplicates of any marker. Therefore it still needs a delicate preprocessing of the input data in which excessive copies of unbalanced markers have to be removed.

In this paper we present an algorithm solving the genomic distance problem for *natural* genomes, in which any marker may occur an arbitrary number of times. Our method is based on a new graph data structure, the *multi-relational diagram*, that allows an elegant extension of the ILP by Shao, Lin and Moret to count *runs* of markers that are under- or over-represented in one genome with respect to the other and need to be inserted or deleted, respectively. With this extension, previous restrictions on the genome configurations are lifted, for the first time enabling an uncompromising rearrangement analysis. Any marker sequence can directly be used for the distance calculation.

The evaluation of our approach shows that it can be used to analyze genomes with up to a few ten thousand markers, which we demonstrate on simulated and real data.

Keywords: comparative genomics · genome rearrangement · DCJ-indel distance

1 Introduction

The study of genome rearrangements has a long tradition in comparative genomics. A central question is how many (and what kind of) mutations have occurred between the genomic sequences of two individual genomes. In order to avoid disturbances due to minor local effects, often the basic units in such comparisons are syntenic regions identified between the genomes under study, much larger than the individual DNA bases. We refer to such regions as *genomic markers*, or simply *markers*, although often one also finds the term *genes*.

Following the initial statement as an edit distance problem [16], a comprehensive trail of literature has addressed the problem of computing the number of rearrangements between two genomes in the past 25 years. In a seminal paper in 1995, Hannenhalli and Pevzner [12] introduced the first polynomial time algorithm for the computation of the inversion distance of transforming one chromosome into another one by means of segmental inversions. Later, the same authors generalized their results to the HP model [11] which is capable of handling multi-chromosomal genomes and accounts for additional genome rearrangements. Another breakthrough was the introduction of the double cut and join (DCJ) model [2, 20], that is able to capture many genome rearrangements and whose genomic distance is computable in linear time. The model is based on a simple operation in which the genome sequence is cut twice between two consecutive markers and re-assembled by joining the resulting four loose cut-ends in a different combination.

A prerequisite for applying the DCJ model in practice to study rearrangements in genomes of two related species is that their genomic marker sets must be identical and that any marker occurs exactly once in each genome. This severely limits its applicability in practice. Linear time extensions of the DCJ model allow markers to occur in only one of the two genomes, computing a genomic distance that minimizes the sum of DCJ and insertion/deletion (indel) events [5, 9]. Still, markers are required to be *singleton*, i.e., no duplicates can occur. When duplicates are allowed, the problem is more intricate and all approaches proposed so far are NP-hard, see for instance [1, 6, 7, 14, 17, 18]. From the practical side, more recently, Shao *et al.* [18] presented an integer linear programming (ILP) formulation for computing the DCJ distance in presence of duplicates, but restricted to *balanced genomes*, where both genomes have equal numbers of duplicates.

In this paper we present the first feasible¹ exact algorithm for solving the NP-hard problem of computing the distance under a general genome model where any marker may occur an arbitrary number of times in any of the two genomes, called *natural genomes*. Specifically, we adopt the *maximal matches* model where only markers appearing more often in one genome than in the other can be deleted or inserted. Our ILP formulation is based on the one from Shao *et al.* [18], but with an efficient extension that allows to count *runs* of markers that are under- or over-represented in one genome with respect to the other, so that the pre-existing model of minimizing the distance allowing DCJ and indel operations [5] can be adapted to our problem. With this extension, once we have the genome markers, no other restriction on the genome configurations is imposed.

The evaluation of our approach shows that it can be used to analyze genomes with up to a few ten thousand markers, provided the number of duplicates is not too large. The complete source code of our ILP implementation and the simulation software used for generating the benchmarking data in Section 4.2 are available from <https://gitlab.ub.uni-bielefeld.de/gi/ding>.

¹ Similar results are claimed to be given in a recent paper by Lyubetsky *et al.* [13], but we were unable to understand their ILP formulation and run their implementation. We compared the performances by running our formulation with the two small examples given in that paper [13, p.8], both with less than 12 markers per genome including duplicates. While they report “about 1.5h” and “about 3h”, we can solve them in less than 20ms each.

2 Preliminaries

A *genome* is a set of *chromosomes* and each chromosome can be linear or circular. Each *marker* in a chromosome is an oriented DNA fragment. The representation of a marker m in a chromosome can be the symbol m itself, if it is read in direct orientation, or the symbol \overline{m} , if it is read in reverse orientation. We represent a chromosome S of a genome A by a string s , obtained by the concatenation of all symbols in S , read in any of the two directions. If S is circular, we can start to read it at any marker and the string s is flanked by parentheses.

Given two genomes A and B , let \mathcal{U} be the set of all markers that occur in both genomes. For each marker $m \in \mathcal{U}$, let $\Phi_A(m)$ be the number of occurrences of m in genome A and $\Phi_B(m)$ be the number of occurrences of m in genome B . We can then define $\Delta\Phi(m) = \Phi_A(m) - \Phi_B(m)$. If both $\Phi_A(m) > 0$ and $\Phi_B(m) > 0$, m is called a *common marker*. We denote by $\mathcal{G} \subseteq \mathcal{U}$ the set of common markers of A and B . The markers in $\mathcal{U} \setminus \mathcal{G}$ are called *exclusive markers*. For example, if we have two unichromosomal linear genomes $A = \{132\overline{5}\overline{4}354\}$ and $B = \{1623173413\}$, then $\mathcal{U} = \{1, 2, 3, 4, 5, 6, 7\}$ and $\mathcal{G} = \{1, 2, 3, 4\}$. Furthermore, $\Delta\Phi(1) = 1 - 3 = -2$, $\Delta\Phi(2) = 1 - 1 = 0$, $\Delta\Phi(3) = 2 - 3 = -1$, $\Delta\Phi(4) = 2 - 1 = 1$, $\Delta\Phi(5) = 2$, and $\Delta\Phi(6) = \Delta\Phi(7) = -1$.

2.1 The DCJ-indel model

A genome can be transformed or *sorted* into another genome with the following types of mutations:

- A *double-cut-and-join* (DCJ) is the operation that cuts a genome at two different positions (possibly in two different chromosomes), creating four open ends, and joins these open ends in a different way. This can represent many different rearrangements, such as inversions, translocations, fusions and fissions. For example, a DCJ can cut linear chromosome $12\overline{4}\overline{3}56$ before and after $\overline{4}\overline{3}$, creating the segments $12\bullet$, $\bullet\overline{4}\overline{3}\bullet$ and $\bullet56$, where the symbol \bullet represents the open ends. By joining the first with the third and the second with the fourth open end, we invert $\overline{4}\overline{3}$ and obtain 123456 .
- Since the genomes can have distinct multiplicity of markers, we also need to consider *insertions* and *deletions* of segments of contiguous markers [5, 9, 21]. We refer to insertions and deletions collectively as *indels*. For example, the deletion of segment 5262 from linear chromosome 12352624 results in 1234 . Indels have two restrictions: (i) only markers that have positive $\Delta\Phi$ can be deleted; and (ii) only markers that have negative $\Delta\Phi$ can be inserted.

In this paper, we are interested in computing the *DCJ-indel distance* between two genomes A and B , that is denoted by $d_{DCJ}^{id}(A, B)$ and corresponds to the minimum number of DCJs and indels required to sort A into B . We separate the instances of the problem in three types:

1. *Singular genomes*: the genomes contain no duplicate markers, that is, each common marker² is singular in each genome. Formally, we have that, for each $m \in \mathcal{G}$, $\Phi_A(m) = \Phi_B(m) = 1$. The distance between singular genomes can be easily computed in linear time [2, 5, 9].
2. *Balanced genomes*: the genomes contain no exclusive markers, but can have duplicates, and the number of duplicates in each genome is the same. Formally, we have $\mathcal{U} = \mathcal{G}$ and, for each $m \in \mathcal{U}$, $\Phi_A(m) = \Phi_B(m)$. Computing the distance for this set of instances is NP-hard, and an ILP formulation was given in [18].
3. *Natural genomes*: these genomes can have exclusive markers and duplicates, with no restrictions on the number of copies. Since these are generalizations of balanced genomes, computing the distance for this set of instances is also NP-hard. In the present work we present an efficient ILP formulation for computing the distance in this case.

² The exclusive markers are not restricted to be singular, because it is mathematically trivial to transform them into singular markers when they occur in multiple copies.

2.2 DCJ-indel distance of singular genomes

First we recall the problem when common duplicates do not occur, that is, when we have singular genomes. We will summarize the linear time approach to compute the DCJ-indel distance in this case that was presented in [5], already adapted to the notation required for presenting the new results of this paper.

Relational diagram. For computing a genomic distance it is useful to represent the relation between two genomes in some graph structure [2, 3, 5, 10, 11]. Here we adopt a variation of it defined as follows. For each marker m , denote its two extremities by m^t (tail) and m^h (head). Given two singular genomes A and B , the *relational diagram* $R(A, B)$ has a set of vertices $V = V(A) \cup V(B)$, where $V(A)$ has a vertex for each extremity of each marker of genome A and $V(B)$ has a vertex for each extremity of each marker of genome B . Due to the 1-to-1 correspondence between the vertices of $R(A, B)$ and the occurrences of marker extremities in A and B , we can identify each extremity with its corresponding vertex. It is convenient to represent vertices in $V(A)$ in an upper line, respecting the order in which they appear in each chromosome of A , and the vertices in $V(B)$ in a lower line, respecting the order in which they appear in each chromosome of B .

If the marker extremities γ_1 and γ_2 are adjacent in a chromosome of A , we have an *adjacency edge* connecting them. Similarly, if the marker extremities γ'_1 and γ'_2 are adjacent in a chromosome of B , we have an adjacency edge connecting them. Marker extremities located at chromosome ends are called *telomeres* and are not connected to any adjacency edge. In contrast, each extremity that is not a telomere is connected to exactly one adjacency edge. Denote by E_{adj}^A and by E_{adj}^B the adjacency edges in A and in B . In addition, for each common marker $m \in \mathcal{G}$, we have two *extremity edges*, one connecting the vertex m^h from $V(A)$ to the vertex m^h from $V(B)$ and the other connecting the vertex m^t from $V(A)$ to the vertex m^t from $V(B)$. Denote by E_γ the set of extremity edges. Finally, for each exclusive marker $q \in \mathcal{U} \setminus \mathcal{G}$, we have an *indel edge* connecting q^t to q^h (of the same occurrence of q). Denote by E_{id}^A and by E_{id}^B the indel edges in A and in B . Each vertex is then connected either to an extremity or to an indel edge.

All vertices have degree one or two, therefore $R(A, B)$ is a simple collection of cycles and paths. A path that has one endpoint in genome A and the other in genome B is called an *AB-path*. In the same way, both endpoints of an *AA-path* are in A and both endpoints of a *BB-path* are in B . Moreover, a path (respect. cycle) of $R(A, B)$ composed exclusively of indel and adjacency edges in one of the two genomes corresponds to a whole linear (respect. circular) chromosome and is called a *linear* (respect. *circular*) *singleton* in that genome. Actually, linear singletons are particular cases of *AA-paths* and *BB-paths*. An example of a relational diagram is given in Fig. 1.

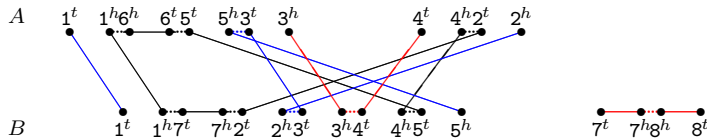


Fig. 1. For genomes $A = \{1\bar{6}53, 42\}$ and $B = \{172345, 7\bar{8}\}$, the relational diagram contains one cycle, two *AB-paths* (represented in blue), one *AA-path* and one *BB-path* (both represented in red). Short dotted horizontal edges are adjacency edges, long horizontal edges are indel edges, top-down edges are extremity edges.

The numbers of telomeres and of *AB-paths* in $R(A, B)$ are even. The *DCJ-cost* [5] of a DCJ operation ρ , denoted by $\|\rho\|$, is defined as follows. If it either increases the number of cycles by one, or the number of *AB-paths* by two, ρ is *optimal* and has $\|\rho\| = 0$. If it does not affect the number of cycles and *AB-paths* in the diagram, ρ is *neutral* and has $\|\rho\| = 1$. If it either decreases the number of cycles by one, or the number of *AB-paths* by two, ρ is *counter-optimal* and has $\|\rho\| = 2$.

Runs and indel-potential. The approach that uses DCJ operations to group exclusive markers for minimizing indels depends on the following concepts (illustrated in Fig. 4 in Appendix A).

Given two genomes A and B and a component C of $R(A, B)$, a *run* [5] is a maximal subpath of C , in which the first and the last edges are indel edges, and all indel edges belong to the same genome. It can be an \mathcal{A} -run when its indel edges are in genome A , or a \mathcal{B} -run when its indel edges are in genome B . We denote by $\Lambda(C)$ the number of runs in component C . If $\Lambda(C) \geq 0$ the component C is said to be *indel-enclosing*, otherwise $\Lambda(C) = 0$ and C is said to be *indel-free*.

While sorting components separately with optimal DCJs only, runs can be accumulated and merged together [5]. The *indel-potential* of a component C , denoted by $\lambda(C)$, is the minimum number of runs derived from C after this process and can be directly computed from $\Lambda(C)$:

$$\lambda(C) = \begin{cases} 0, & \text{if } \Lambda(C) = 0 \quad (C \text{ is indel-free}); \\ \left\lceil \frac{\Lambda(C)+1}{2} \right\rceil, & \text{if } \Lambda(C) \geq 1 \quad (C \text{ is indel-enclosing}). \end{cases}$$

Let λ_0 and λ_1 be, respectively, the sum of the indel-potentials for the components of the relational diagram before and after a DCJ ρ . The *indel-cost* of ρ is then $\Delta\lambda(\rho) = \lambda_1 - \lambda_0$, and the DCJ-indel cost of ρ is defined as $\Delta d(\rho) = \|\rho\| + \Delta\lambda(\rho)$. While sorting components separately, it has been shown that by using neutral or counter-optimal DCJs one can never achieve $\Delta d < 0$ [5]. This gives the following result:

Lemma 1 (from [2,5]). *Given two singular genomes A and B , whose relational diagram $R(A, B)$ has c cycles and i AB -paths, we have*

$$d_{DCJ}^{id}(A, B) \leq |\mathcal{G}| - c - \frac{i}{2} + \sum_{C \in R(A, B)} \lambda(C).$$

Distance of circular genomes. For singular circular genomes, the graph $R(A, B)$ is composed of cycles only. In this case the upper bound given by Lemma 1 is tight and leads to a simplified formula:

$$d_{DCJ}^{id}(A, B) = |\mathcal{G}| - c + \sum_{C \in R(A, B)} \lambda(C).$$

Recombinations and linear genomes. For singular linear genomes, the upper bound given by Lemma 1 is achieved when the components of $R(A, B)$ are sorted separately. However, there are optimal or neutral DCJ operations, called *recombinations*, that act on two paths and have $\Delta d < 0$. Such path recombinations are said to be *deducting*. The total number of types of deducting recombinations is relatively small. By exhaustively exploring the space of recombination types, it is possible to identify groups of chained recombinations (listed in Table 4 of Appendix A), so that the sources of each group are the original paths of the graph. In other words, a path that is a resultant of a group is never a source of another group. This results in a greedy approach (detailed in Appendix A) that optimally finds the value $\delta \geq 0$ to be deducted.

Theorem 1 (adapted from [5]). *Given two singular linear genomes A and B , whose relational diagram $R(A, B)$ has c cycles and i AB -paths, and letting δ be the value obtained by maximizing deductions of path recombinations, we have*

$$d_{DCJ}^{id}(A, B) = |\mathcal{G}| - c - \frac{i}{2} + \sum_{C \in R(A, B)} \lambda(C) - \delta.$$

3 DCJ-indel distance of natural genomes

In this work we are interested in comparing two natural genomes A and B . First we observe that it is possible to transform A and B into *matched* singular genomes A^\dagger and B^\dagger as follows. For each common marker $m \in \mathcal{G}$, if $\Phi_A \leq \Phi_B$, we should determine which occurrence of m in B matches each occurrence of m in A , or if $\Phi_B < \Phi_A$, which occurrence of m in A matches each occurrence of m in B . The matched occurrences receive the same identifier (for example, by adding the same *index*) in A^\dagger and in B^\dagger . Examples are given in Fig. 2 (top). Observe that, after this procedure, the number of common markers between any pair of matched genomes A^\dagger and B^\dagger is

$$n_* = \sum_{m \in \mathcal{G}} \min\{\Phi_A(m), \Phi_B(m)\}.$$

Let \mathbb{M} be the set of all possible pairs of matched singular genomes obtained from natural genomes A and B . The DCJ-indel distance of A and B is then defined as

$$d_{DCJ}^{id}(A, B) = \min_{(A^\dagger, B^\dagger) \in \mathbb{M}} \{d_{DCJ}^{id}(A^\dagger, B^\dagger)\}.$$

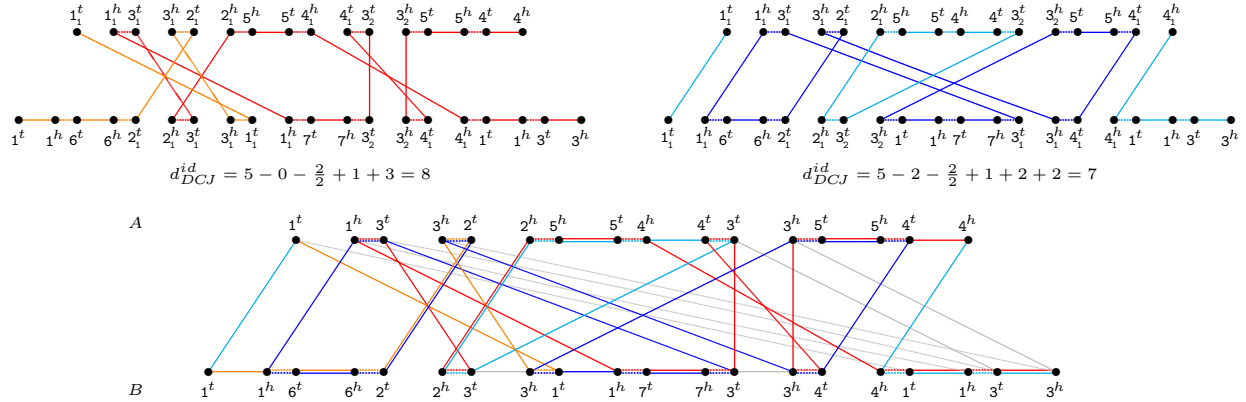


Fig. 2. Natural genomes $A = 1325\bar{4}354$ and $B = 1623173413$ can give rise to many distinct pairs of matched singular genomes. The relational diagrams of two of these pairs are represented here, in the top part. In the bottom part we show the multi-relational diagram $MR(A, B)$. The decomposition that gives the diagram on the top-left is represented in red/orange. Similarly, the decomposition that gives the diagram on the top-right is represented in blue/cyan. Edges that are in both decompositions have two colors.

3.1 Multi-relational diagram

While the original relational diagram clearly depends on the singularity of common markers, when they appear in multiple copies we can obtain a data structure that integrates the properties of all possible relational diagrams of matched genomes. The *multi-relational diagram* $MR(A, B)$ of two natural genomes A and B also has a set $V(A)$ with a vertex for each of the two extremities of each marker occurrence of genome A and a set $V(B)$ with a vertex for each of the two extremities of each marker occurrence of genome B .

Again, sets E_{adj}^A and E_{adj}^B contain adjacency edges connecting adjacent extremities of markers in A and in B . But here the set E_γ contains, for each marker $m \in \mathcal{G}$, an extremity edge connecting each vertex in $V(A)$ that represents an occurrence of m^t to each vertex in $V(B)$ that represents an occurrence of m^t , and an extremity edge connecting each vertex in $V(A)$ that represents an occurrence of m^h to each vertex in $V(B)$ that represents an occurrence of m^h . Furthermore, for each marker $m \in \mathcal{U}$ with $\Phi_A(m) > \Phi_B(m)$, the set E_{id}^A contains one indel edge connecting the vertices representing the two extremities of the same occurrence of m in A . Similarly, for each

marker $m' \in \mathcal{U}$ with $\Phi_B(m') > \Phi_A(m')$, the set E_{id}^B contains one indel edge connecting the vertices representing the two extremities of the same occurrence of m' in B . An example of a multi-relational diagram is given in Fig. 2 (bottom).

Consistent decompositions. Note that if A and B are singular genomes, $MR(A, B)$ reduces to the ordinary $R(A, B)$. On the other hand, in the presence of duplicate common markers, $MR(A, B)$ may contain vertices of degree larger than two. A *decomposition* is a collection of vertex-disjoint *components*, that can be cycles and/or paths, covering all vertices of $MR(A, B)$. There can be multiple ways of selecting a decomposition, and we need to find one that allows to match occurrences of a marker in genome A with occurrences of the same marker in genome B .

Let $m_{(A)}$ and $m_{(B)}$ be, respectively, occurrences of the same marker m in genomes A and B . The extremity edge that connects $m_{(A)}^h$ to $m_{(B)}^h$ and the extremity edge that connects $m_{(A)}^t$ to $m_{(B)}^t$ are called *siblings*. A set $E_D \subseteq E_\gamma$ is a *sibling-set* if it is exclusively composed of disjoint pairs of siblings. Thus, a *maximal* sibling-set E_D corresponds to a maximal matching of occurrences of common markers in both genomes.

The sets of adjacency edges E_{adj}^A and E_{adj}^B and subsets of indel edges $E_1 \subseteq E_{id}^A$ and $E_2 \subseteq E_{id}^B$ unambiguously connect the components derived from a maximal sibling-set E_D into a collection D of vertex-disjoint cycles and paths, that cover all vertices of $MR(A, B)$. Such a collection D induced by E_D is said to be a *consistent decomposition* of $MR(A, B)$ and allows us to compute the value

$$d_{DCJ}^{id}(D) = n_* - c_D - \frac{i_D}{2} + \sum_{C \in D} \lambda(C) - \delta_D,$$

where c_D and i_D are the numbers of cycles and AB -paths in D , respectively, and δ_D is the optimal deduction of recombinations of paths from D . Since n_* is constant for any consistent decomposition, we can separate the part of the formula that depends on D , called *weight* of D :

$$w(D) = c_D + \frac{i_D}{2} - \sum_{C \in D} \lambda(C) + \delta_D.$$

Theorem 2. *Given two natural genomes A and B , the DCJ-indel distance of A and B can be computed by the following equation:*

$$d_{DCJ}^{id}(A, B) = \min_{D \in \mathbb{D}} \{d_{DCJ}^{id}(D)\} = n_* - \max_{D \in \mathbb{D}} \{w(D)\},$$

where \mathbb{D} is the set of all consistent decompositions of $MR(A, B)$.

Proof. Since a consistent decomposition allows to match duplicates in both genomes, it is clear that $d_{DCJ}^{id}(A, B) \leq \min_{D \in \mathbb{D}} \{d_{DCJ}^{id}(D)\}$. Now, assume that $d_{DCJ}^{id}(A, B) < \min_{D \in \mathbb{D}} \{d_{DCJ}^{id}(D)\}$. By definition, $d_{DCJ}^{id}(A, B)$ corresponds to an optimal rearrangement scenario from A to some B and therefore implies a matching between the markers of A and the markers of B that gives rise to a consistent decomposition D' of $MR(A, B)$ such that $d_{DCJ}^{id}(D') < \min_{D \in \mathbb{D}} \{d_{DCJ}^{id}(D)\}$, which is a contradiction. \square

A consistent decomposition D such that $d_{DCJ}^{id}(D) = d_{DCJ}^{id}(A, B)$ is said to be *optimal*. Computing the DCJ-indel distance between two natural genomes A and B , or, equivalently, finding an optimal consistent decomposition of $MR(A, B)$ is an NP-hard problem. In Section 4 we will describe an efficient ILP formulation to solve it. Before that, we need to introduce a transformation of $MR(A, B)$ that is necessary for the ILP.

3.2 Capping

The ends of linear chromosomes produce some difficulties for the decomposition. Fortunately there is an elegant technique to overcome this problem, called *capping* [11]. It consists of modifying the genomes by adding *artificial* singular common markers, also called *caps*, that circularize all linear chromosomes, so that their relational diagram is composed of cycles only, but, if the capping is optimal, the genomic distance is preserved.

Singular genomes. An optimal capping of singular genomes can be obtained by finding caps that properly link the sources of each recombination group into a single cycle. Indeed, in Table 6 (Appendix B) we give a linking that achieves the optimal Δd for each recombination group, followed by the optimal linking of remaining paths. By greedily linking the paths following a top-down order of this table we clearly obtain an optimal capping that transforms A and B into circular genomes A_\circ and B_\circ with $d_{DCJ}^{id}(A_\circ, B_\circ) = d_{DCJ}^{id}(A, B)$. Appendix B also proves the following theorem.

Theorem 3. *Let κ_A and κ_B be, respectively, the total numbers of linear chromosomes in singular genomes A and B . The number of caps in the optimal capping given by Table 6 (Appendix B) is*

$$p_* = \max\{\kappa_A, \kappa_B\}$$

and the number of artificial adjacencies between caps is $a_ = |\kappa_A - \kappa_B|$.*

Capped multi-relational diagram. As illustrated in Figure 9 (of Appendix B), we can transform $MR(A, B)$ into the *capped multi-relational diagram* $MR_\circ(A, B)$ as follows. First we need to create $4p_*$ new vertices, named $\circ_A^1, \circ_A^2, \dots, \circ_A^{2p_*}$ and $\circ_B^1, \circ_B^2, \dots, \circ_B^{2p_*}$, each one representing a *cap extremity*. Each of the $2\kappa_A$ telomeres of A is connected by an adjacency edge to a distinct cap extremity among $\circ_A^1, \circ_A^2, \dots, \circ_A^{2\kappa_A}$. Similarly, each of the $2\kappa_B$ telomeres of B is connected by an adjacency edge to a distinct cap extremity among $\circ_B^1, \circ_B^2, \dots, \circ_B^{2\kappa_B}$. Moreover, if $\kappa_A < \kappa_B$, for $i = 2\kappa_A + 1, 2\kappa_A + 3, \dots, 2\kappa_B - 1$, connect \circ_A^i to \circ_A^{i+1} by an *artificial adjacency edge*. Otherwise, if $\kappa_B < \kappa_A$, for $j = 2\kappa_B + 1, 2\kappa_B + 3, \dots, 2\kappa_A - 1$, connect \circ_B^j to \circ_B^{j+1} by an artificial adjacency edge. All these new adjacency edges and artificial adjacency edges are added to E_{adj}^A and E_{adj}^B , respectively.

We also connect each \circ_A^i , $1 \leq i \leq 2p_*$, by a *cap extremity edge* to each \circ_B^j , $1 \leq j \leq 2p_*$, and denote by E_\circ the set of cap extremity edges. A set $E'_D \subseteq E_\circ$ is a *capping-set* if it is exclusively composed of disjoint edges. A consistent decomposition D of $MR_\circ(A, B)$ is induced by a maximal sibling-set $E_D \subseteq E_\gamma$ and a maximal capping-set $E'_D \subseteq E_\circ$ and is composed of vertex disjoint cycles covering all vertices of $MR_\circ(A, B)$. We then have $d_{DCJ}^{id}(D) = n_* + p_* - w(D)$, where the weight of D can be computed by the simpler formula

$$w(D) = c_D - \sum_{C \in D} \lambda(C).$$

Finally, if \mathbb{D}_\circ is the set of all consistent decompositions of $MR_\circ(A, B)$, we have

$$d_{DCJ}^{id}(A, B) = n_* + p_* - \max_{D \in \mathbb{D}_\circ} \{w(D)\}.$$

Note that the $2p_*$ cap extremities added to each genome correspond to p_* implicit caps. Furthermore, the number of artificial adjacency edges added to the genome with less linear chromosomes is $a_* = |\kappa_A - \kappa_B|$. Since each pair of matched singular genomes $(A^\dagger, B^\dagger) \in \mathbb{M}$ can be optimally capped with this number of caps and artificial adjacencies, it is clear that at least one optimal capping of each (A^\dagger, B^\dagger) corresponds to a consistent decomposition $D \in \mathbb{D}_\circ$.

4 An algorithm to compute the DCJ-indel distance of natural genomes

An ILP formulation for computing the distance of two balanced genomes A and B was given by Shao *et al.* in [18]. In this section we describe an extension of that formulation for computing the DCJ-indel distance of natural genomes A and B , based on consistent cycle decompositions of $MR_o(A, B)$. The main difference is that here we need to address the challenge of computing the indel-potential $\lambda(C)$ for each cycle C of each decomposition. This task is easier to accomplish by redesigning the formula that computes the indel-potential, obtaining one that is split into a part that simply tests whether C is indel-enclosing and a part that depends on the number of *transitions* (from a run in one genome to a run in the other genome), denoted by $\aleph(C)$. Observe that, if $\Lambda(C) \leq 1$, we have $\aleph(C) = 0$, otherwise $\aleph(C) = \Lambda(C)$.

Proposition 1. *Given the function $r(C)$ defined as $r(C) = 1$ if $\Lambda(C) \geq 1$, otherwise $r(C) = 0$, the indel-potential $\lambda(C)$ can be computed from the number of transitions $\aleph(C)$ with the formula*

$$\lambda(C) = \frac{\aleph(C)}{2} + r(C).$$

Now, given that $c_D^r = \sum_{C \in D} r(C)$ is the number of indel-enclosing cycles in D , while the number of indel-free cycles is $c_D^{\tilde{r}} = c_D - c_D^r$, we need to find a consistent decomposition D of $MR_o(A, B)$, maximizing its weight:

$$w(D) = c_D - \sum_{C \in D} \lambda(C) = c_D - \sum_{C \in D} \left(\frac{\aleph(C)}{2} + r(C) \right) = c_D - \left(c_D^r + \sum_{C \in D} \frac{\aleph(C)}{2} \right) = c_D^{\tilde{r}} - \sum_{C \in D} \frac{\aleph(C)}{2}.$$

4.1 ILP formulation

Our formulation (shown in Algorithm 1) searches for an optimal consistent cycle decomposition of $MR_o(A, B) = (V, E)$, where the set of edges E is the union of all disjoint sets of the distinct types of edges, $E = E_\gamma \cup E_o \cup E_{adj}^A \cup E_{adj}^B \cup E_{id}^A \cup E_{id}^B$.

In the first part we use the same strategy as the one of Shao *et al.* [18]. A binary variable x_e (D.01) is introduced for every edge e , indicating whether e is part of the computed decomposition. Constraint C.01 ensures that adjacency edges are in all decompositions, Constraint C.02 ensures that each vertex of each decomposition has degree 2, and Constraint C.03 ensures that an extremity edge is only selected together with its sibling. Counting the number of cycles in each decomposition is achieved by assigning a unique identifier i to each vertex v_i that is then used to label each cycle with the numerically smallest identifier of any contained vertex (see Constraint C.04, Domain D.02). A vertex v_i is then marked by variable z_i (D.03) as representative of a cycle if its cycle label y_i is equal to i (C.06). However, unlike Shao *et al.*, we permit each variable y_i to take on value 0 which, by Constraint C.05, will be enforced whenever the corresponding cycle is indel-enclosing. Since the smallest label of any vertex is 1 (cf. D.02), any cycle with label 0 will not be counted.

The second part is our extension for counting transitions. We introduce binary variables r_v (D.04) to label runs. To this end, Constraint C.07 ensures that each vertex v is labeled 0 if v is part of an \mathcal{A} -run and otherwise it is labeled 1 indicating its participation in a \mathcal{B} -run. Transitions between \mathcal{A} - and \mathcal{B} -runs in a cycle are then recorded by binary variable t_e (D.05). If a transition occurs between any neighboring pair of vertices $u, v \in V$ of a cycle, Constraint C.08 causes transition variable $t_{\{u,v\}}$ to be set to 1. We avoid an excess of co-optimal solutions by canonizing the locations in which such transitions may take place. More specifically, Constraint C.10 prohibits label changes in adjacencies not directly connected to an indel and Constraint C.09 in edges other than adjacencies of genome A .

The objective of our ILP is to maximize the weight of a consistent decomposition, that is equivalent to maximizing the number of indel-free cycles, counted by the sum over variables z_i , while simultaneously minimizing the number of transitions in indel-enclosing cycles, calculated by half the sum over variables t_e .

Algorithm 1 ILP for the computation of the DCJ-indel distance of natural genomes

Objective:

$$\text{Maximize} \quad \sum_{1 \leq i \leq |V|} z_i - \frac{1}{2} \sum_{e \in E} t_e$$

Constraints:

(C.01) $x_e = 1$	$\forall e \in E_{adj}^A \cup E_{adj}^B$	(C.07) $r_v \leq 1 - x_{\{u,v\}}$	$\forall \{u,v\} \in E_{id}^A,$
(C.02) $\sum_{\{u,v\} \in E} x_{\{u,v\}} = 2$	$\forall u \in V$	$r_{v'} \geq x_{\{u',v'\}}$	$\forall \{u',v'\} \in E_{id}^B$
(C.03) $x_e = x_d$	$\forall e, d \in E_\gamma$ such that e and d are siblings	(C.08) $t_{\{u,v\}} \geq r_v - r_u - (1 - x_{\{u,v\}})$	$\forall \{u,v\} \in E$
(C.04) $y_i \leq y_j + i(1 - x_{\{v_i,v_j\}})$	$\forall \{v_i,v_j\} \in E,$	(C.09) $t_e = 0$	$\forall e \in E \setminus E_{adj}^A$
(C.05) $y_i \leq i(1 - x_{\{v_i,v_j\}})$	$\forall \{v_i,v_j\} \in E_{id}^A \cup E_{id}^B$	(C.10) $\sum_{\{v,w\} \in E_{id}^A} x_{\{v,w\}} - t_{\{u,v\}} \geq 0$	$\forall \{u,v\} \in E_{adj}^A$
(C.06) $i \cdot z_i \leq y_i$	$\forall 1 \leq i \leq V $		

Domains:

(D.01) $x_e \in \{0, 1\} \quad \forall e \in E$	(D.04) $r_v \in \{0, 1\} \quad \forall v \in V$
(D.02) $0 \leq y_i \leq i \quad \forall 1 \leq i \leq V $	(D.05) $t_e \in \{0, 1\} \quad \forall e \in E$
(D.03) $z_i \in \{0, 1\} \quad \forall 1 \leq i \leq V $	

4.2 Performance benchmark on simulated data

We implemented the construction of the ILP as a python application (available at <https://gitlab.ub.uni-bielefeld.de/gi/ding>) and used CPLEX as solver. For benchmarking purposes, we applied the ILP to simulated pairs of genomes composed of $\sim 20,000$ marker occurrences. Because the number of duplicate markers has an unlike higher impact on the running time than the number of cycles in the multi-relational diagram, we kept the number of DCJ events fixed to 10,000 and varied parameters that affect the number of duplicates. Further information on the simulation is provided in Appendix C.

Our ILP solves the decomposition problem efficiently for real-sized genomes under small to moderate numbers of duplicate markers: running times for genome pairs with less than 4,000 duplicated markers ($\sim 20\%$ of the genome size) shown in Figure 3 are with few exceptions below one minute and exhibit a linear increase, but running time is expected to boost dramatically with higher numbers of duplicates. To further exploit the conditions under which the ILP is no longer solvable with reasonable compute resources we continued the experiment with even higher amounts of duplicate markers and instructed CPLEX to terminate within 1 hour of computation. We then partitioned the simulated data set into 6 intervals of length 500 according to the observed number of duplicated markers. For each interval, we determined the average number of duplicated marker occurrences as well as the maximal multiplicity of any constructed marker and examined the median *optimality gap*, i.e., the difference in percentage between the best primal and the best dual solution computed within the time limit. The results are shown in Table 1 and emphasize the impact of duplicate markers in running time: below 6,000 duplicate markers, the optimality gap remains small and often our approach computes the exact solution, whereas above that threshold the gap widens very quickly.

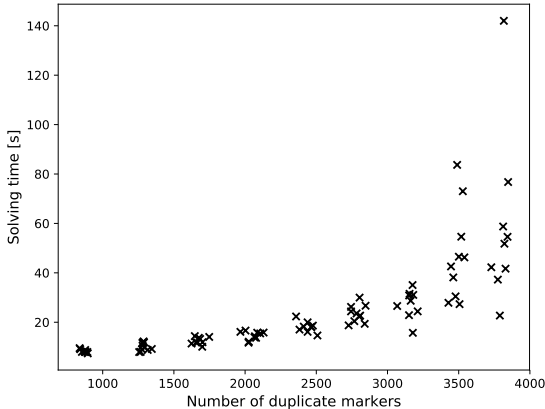


Fig. 3. Solving times using a single CPLEX thread for genomes with varying number of duplicates, totaling 20,000 marker occurrences per genome.

number of dupl. markers	avg. mult. of dupl. markers	max. multi- plicity	median optimality gap (%) [*]
4000..4499	2.16	6	—
4500..4999	2.18	7	—
5000..5499	2.20	8	—
5500..5999	2.23	9	0.03
6000..6499	2.25	7	67.98
6500..6999	2.28	9	656.22

^{*} A dash indicates that all instances could be solved to optimality.

Table 1. Median optimality gap for groups of simulated genome pairs with similar numbers of duplicated markers after 1h of running time.

4.3 Real data analysis

Recently, the first three high-resolution haplotype-resolved human genomes have been published [8]. Here, we demonstrate the applicability of our approach to the study of real data by calculating the DCJ-indel distance between one of these haplotypes (HG00514.h0) and the human reference sequence (GRCh38). After the construction of a genomic marker set, we represented each chromosome of both genomes as marker sequence, with the largest chromosome (chr. 1) comprising close to 18,000 markers. We then ran our ILP for the computation of the DCJ-indel distance on each pair of chromosomes independently. We were able to obtain exact solutions for 17 chromosomes within few minutes. However, the remaining six comparisons did not complete within 12 hours of computation. Still, after that time, their optimality gaps were below 0.2%. The calculated DCJ-indel distances ranged between 3.3% and 11.5% of the length of the marker sequences, with the number of runs accounting for 34% to 78% of the distance. Further details on the data set, the construction of the genomic markers, and the calculated DCJ-indel distances are described in Appendix D.

5 Conclusion

By extending the DCJ-indel model to allow for duplicate markers, we introduced a rearrangement model that is capable of handling *natural genomes*, i.e., genomes that contain shared, individual, and duplicated markers. In other words, under this model genomes require no further processing nor manipulation once genomic markers and their homologies are inferred. The DCJ-indel distance of natural genomes being NP-hard, we presented a fast method for its calculation in form of an *integer linear program* (ILP). Our program is capable of handling real-sized genomes, as evidenced in simulation and real data experiments. It can be applied universally in comparative genomics and enables uncompromising analyses of genome rearrangements. We hope that such analyses will provide further insights into the underlying mutational mechanisms. Conversely, we expect the here presented model to be extended and specialized in future to reflect the insights gained by these analyses.

References

1. Angibaud, S., Fertin, G., Rusu, I., Thévenin, A., Vialette, S.: On the approximability of comparing genomes with duplicates. *J. Graph Algorithms Appl.* **13**(1), 19–53 (2009), (A preliminary version appeared in Proc. of WALCOM (2008).)
2. Bergeron, A., Mixtacki, J., Stoye, J.: A unifying view of genome rearrangements. In: Proceedings of the 6th International Conference on Algorithms in Bioinformatics (WABI 2006). LNBI, vol. 4175, pp. 163–173. Springer Verlag (2006)
3. Braga, M.D.V.: An overview of genomic distances modeled with indels. In: Proceedings of the Conference on Computability in Europe (CiE 2013). LNCS, vol. 7921, pp. 22–31. Springer Verlag (2013)
4. Braga, M.D.V., Stoye, J.: The solution space of sorting by DCJ. *Journal of Computational Biology* **17**(9), 1145–1165 (2010), (A preliminary version appeared in Proc. of Recomb-CG (2009).)
5. Braga, M.D.V., Willing, E., Stoye, J.: Double cut and join with insertions and deletions. *Journal of Computational Biology* **18**(9), 1167–1184 (2011), (A preliminary version appeared in Proc. of WABI (2010).)
6. Bryant, D.: The complexity of calculating exemplar distances. In: Sankoff, D., Nadeau, J.H. (eds.) *Comparative Genomics*, pp. 207–211. Kluwer Academic Publishers (2000)
7. Bulteau, L., Jiang, M.: Inapproximability of (1,2)-exemplar distance. *IEEE/ACM Trans. Comput. Biol. Bioinf.* **10**(6), 1384–1390 (2013), (A preliminary version appeared in Proc. of ISBRA (2012).)
8. Chaisson, M.J.P., Sanders, A.D., Zhao, X., Malhotra, A., Porubsky, D., Rausch, T., Gardner, E.J., Rodriguez, O.L., Guo, L., Collins, R.L., Fan, X., Wen, J., Handsaker, R.E., Fairley, S., Kronenberg, Z.N., Kong, X., Hormozdizari, F., Lee, D., Wenger, A.M., Hastie, A.R., Antaki, D., Anantharaman, T., Audano, P.A., Brand, H., Cantsilieris, S., Cao, H., Cerveira, E., Chen, C., Chen, X., Chin, C.S., Chong, Z., Chuang, N.T., Lambert, C.C., Church, D.M., Clarke, L., Farrell, A., Flores, J., Galeev, T., Gorkin, D.U., Gujral, M., Guryev, V., Heaton, W.H., Korlach, J., Kumar, S., Kwon, J.Y., Lam, E.T., Lee, J.E., Lee, J., Lee, W.P., Lee, S.P., Li, S., Marks, P., Viaud-Martinez, K., Meiers, S., Munson, K.M., Navarro, F.C.P., Nelson, B.J., Nodzak, C., Noor, A., Kyriazopoulou-Panagiotopoulou, S., Pang, A.W.C., Qiu, Y., Rosanio, G., Ryan, M., Stutz, A., Spierings, D.C.J., Ward, A., Welch, A.E., Xiao, M., Xu, W., Zhang, C., Zhu, Q., Zheng-Bradley, X., Lowy, E., Yakneen, S., McCarroll, S., Jun, G., Ding, L., Koh, C.L., Ren, B., Flicek, P., Chen, K., Gerstein, M.B., Kwok, P.Y., Lansdorp, P.M., Marth, G.T., Sebat, J., Shi, X., Bashir, A., Ye, K., Devine, S.E., Talkowski, M.E., Mills, R.E., Marschall, T., Korbel, J.O., Eichler, E.E., Lee, C.: Multi-platform discovery of haplotype-resolved structural variation in human genomes. *Nature Communications* **10**(1), 1–16 (Apr 2019)
9. Compeau, P.E.C.: DCJ-indel sorting revisited. *Algorithms for Molecular Biology* **8**, 6 (2013), (A preliminary version appeared in Proc. of WABI (2012).)
10. Friedberg, R., Darling, A.E., Yancopoulos, S.: Genome rearrangement by the double cut and join operation. In: Keith, J.M. (ed.) *Bioinformatics, Volume I: Data, Sequence Analysis, and Evolution, Methods in Molecular Biology*, vol. 452, pp. 385–416. Humana Press (2008)
11. Hannenhalli, S., Pevzner, P.A.: Transforming men into mice (polynomial algorithm for genomic distance problem). In: Proceedings of the 36th Annual Symposium of the Foundations of Computer Science (FOCS 1995). pp. 581–592. IEEE Press (1995)
12. Hannenhalli, S., Pevzner, P.A.: Transforming cabbage into turnip: polynomial algorithm for sorting signed permutations by reversals. *Journal of the ACM* **46**(1), 1–27 (1999), (A preliminary version appeared in Proc. of STOC (1995).)
13. Lyubetsky, V., Gershgorin, R., Gorbunov, K.: Chromosome structures: reduction of certain problems with unequal gene content and gene paralogs to integer linear programming. *BMC Bioinformatics* **18**, 537 (2017)
14. Martinez, F.V., Feijão, P., Braga, M.D.V., Stoye, J.: On the family-free DCJ distance and similarity. *Algorithms for Molecular Biology* **10**, 13 (2015), (A preliminary version appeared in Proc. of WABI (2014).)
15. Rubert, D., Martinez, F.V.H., Stoye, J., Doerr, D.: Analysis of local genome rearrangement improves resolution of ancestral genomic maps in plants. *BMC Genomics* (2019), (Accepted; Proc. of RECOMB-CG (2019).)
16. Sankoff, D.: Edit distance for genome comparison based on non-local operations. In: Apostolico, A., Crochemore, M., Galil, Z., Manber, U. (eds.) *Proceedings of the Third Annual Symposium on Combinatorial Pattern Matching, CPM 1992*. LNCS, vol. 644, pp. 121–135. Springer Verlag, Berlin (1992)
17. Sankoff, D.: Genome rearrangement with gene families. *Bioinformatics* **15**(11), 909–917 (1999)
18. Shao, M., Lin, Y., Moret, B.M.E.: An exact algorithm to compute the double-cut-and-join distance for genomes with duplicate genes. *J. Comp. Biol.* **22**(5), 425–435 (2015), (A preliminary version appeared in Proc. of RECOMB (2014).)
19. Visnovská, M., Vinař, T., Brejová, B.: DNA Sequence Segmentation Based on Local Similarity. *ITAT* pp. 36–43 (2013)
20. Yancopoulos, S., Attie, O., Friedberg, R.: Efficient sorting of genomic permutations by translocation, inversion and block interchange. *Bioinformatics* **21**(16), 3340–3346 (2005)

21. Yancopoulos, S., Friedberg, R.: DCJ path formulation for genome transformations which include insertions, deletions, and duplications. *Journal of Computational Biology* **16**(10), 1311–1338 (2009), (A preliminary version appeared in *Proc. of RECOMB-CG* (2008).)

A Path recombinations and DCJ-indel distance of singular linear genomes

Here we recall results from [5] that are necessary for proving the contents of Appendix B.

Remember that the indel-potential of a component C depends only on its initial number of runs $\Lambda(C)$ and can be computed by the formula

$$\lambda(C) = \begin{cases} 0, & \text{if } \Lambda(C) = 0; \\ \left\lceil \frac{\Lambda(C)+1}{2} \right\rceil, & \text{if } \Lambda(C) \geq 1. \end{cases}$$

Figure 4 shows a BB -path with 4 runs, and how its indel-potential can be achieved.



Fig. 4. (i) A BB -path with 4 runs. (ii) After an optimal DCJ that creates a new cycle, one A -run is accumulated and two B -runs are merged. Indeed the indel-potential of the original BB -path is three.

A.1 Deducting recombinations

In a recombination, the two paths on which the cuts are applied are called *sources* and the paths obtained after the joinings are called *resultants*. Any recombination whose sources are an AA -path and a BB -path is optimal. A recombination whose sources are two different AB -paths can be either neutral, when the resultants are also AB -paths, or counter-optimal, when the resultants are an AA -path and a BB -path. Any recombination whose sources are an AB -path and an AA - or a BB -path is neutral [4, 5].

Let \mathcal{A} (respectively \mathcal{B}) be a sequence with an odd (≥ 1) number of runs, starting and ending with an A -run (respectively B -run). We can then make any combination of \mathcal{A} and \mathcal{B} , such as \mathcal{AB} , that is a sequence with an even (≥ 2) number of runs, starting with an A -run and ending with a B -run. An empty sequence (with no run) is represented by ε . Then each one of the notations AA_ε , $AA_{\mathcal{A}}$, $AA_{\mathcal{B}}$, $AA_{\mathcal{AB}} \equiv AA_{\mathcal{BA}}$, BB_ε , $BB_{\mathcal{A}}$, $BB_{\mathcal{B}}$, $BB_{\mathcal{AB}} \equiv BB_{\mathcal{BA}}$, AB_ε , $AB_{\mathcal{A}}$, $AB_{\mathcal{B}}$, $AB_{\mathcal{AB}}$ and $AB_{\mathcal{BA}}$ represents a particular type of path (AA , BB or AB) with a particular structure of runs (ε , \mathcal{A} , \mathcal{B} , \mathcal{AB} or \mathcal{BA}). By convention, an AB -path is always read from A to B . These notations were adopted due to the observation that, besides the DCJ type of the recombination (optimal, neutral or counter-optimal), the only properties that matter are whether the paths have an odd or an even number of runs and whether the first run is in genome A or in genome B [5]. An example of a deducting recombination is given in Fig. 5.

The complete set of path recombinations with $\Delta d \leq -1$ is given in Table 2. In Table 3 we also list recombinations with $\Delta d = 0$ that create at least one source of recombinations of Table 2. We denote by \bullet an AB -path that can not be a source of a recombination in Tables 2 and 3, such as AB_ε , $AB_{\mathcal{A}}$ and $AB_{\mathcal{B}}$.

The two sources of a recombination can also be called *partners*. Looking at Table 2 we observe that all partners of $AB_{\mathcal{AB}}$ and $AB_{\mathcal{BA}}$ paths are also partners of $AA_{\mathcal{AB}}$ and $BB_{\mathcal{AB}}$ paths, all partners of $AA_{\mathcal{A}}$ and $AA_{\mathcal{B}}$ paths are also partners of $AA_{\mathcal{AB}}$ paths and all partners of $BB_{\mathcal{A}}$ and $BB_{\mathcal{B}}$ paths are also partners of $BB_{\mathcal{AB}}$ paths. Moreover, in some cases deducting recombinations are *chained*,

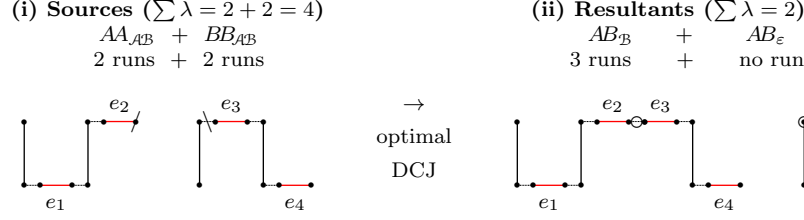


Fig. 5. An optimal recombination with $\Delta d = \Delta \lambda = -2$.

Table 2. Path recombinations that have $\Delta d \leq -1$ and allow the best reuse of the resultants.

sources	resultants	$\Delta \lambda$	$\ \rho\ $	Δd
$AA_{\mathcal{A}\mathcal{B}} + BB_{\mathcal{A}\mathcal{B}}$	$\bullet + \bullet$	-2	0	-2
$AA_{\mathcal{A}\mathcal{B}} + BB_{\mathcal{A}}$	$\bullet + AB_{\mathcal{B}\mathcal{A}}$	-1	0	-1
$AA_{\mathcal{A}\mathcal{B}} + BB_{\mathcal{B}}$	$\bullet + AB_{\mathcal{A}\mathcal{B}}$	-1	0	-1
$AA_{\mathcal{A}} + BB_{\mathcal{A}\mathcal{B}}$	$\bullet + AB_{\mathcal{A}\mathcal{B}}$	-1	0	-1
$AA_{\mathcal{B}} + BB_{\mathcal{A}\mathcal{B}}$	$\bullet + AB_{\mathcal{B}\mathcal{A}}$	-1	0	-1
$AA_{\mathcal{A}} + BB_{\mathcal{A}}$	$\bullet + \bullet$	-1	0	-1
$AA_{\mathcal{B}} + BB_{\mathcal{B}}$	$\bullet + \bullet$	-1	0	-1

sources	resultants	$\Delta \lambda$	$\ \rho\ $	Δd
$AA_{\mathcal{A}\mathcal{B}} + AA_{\mathcal{A}\mathcal{B}}$	$AA_{\mathcal{A}} + AA_{\mathcal{B}}$	-2	+1	-1
$BB_{\mathcal{A}\mathcal{B}} + BB_{\mathcal{A}\mathcal{B}}$	$BB_{\mathcal{A}} + BB_{\mathcal{B}}$	-2	+1	-1
$AA_{\mathcal{A}\mathcal{B}} + AB_{\mathcal{A}\mathcal{B}}$	$\bullet + AA_{\mathcal{A}}$	-2	+1	-1
$AA_{\mathcal{A}\mathcal{B}} + AB_{\mathcal{B}\mathcal{A}}$	$\bullet + AA_{\mathcal{B}}$	-2	+1	-1
$BB_{\mathcal{A}\mathcal{B}} + AB_{\mathcal{A}\mathcal{B}}$	$\bullet + BB_{\mathcal{B}}$	-2	+1	-1
$BB_{\mathcal{A}\mathcal{B}} + AB_{\mathcal{B}\mathcal{A}}$	$\bullet + BB_{\mathcal{A}}$	-2	+1	-1
$AB_{\mathcal{A}\mathcal{B}} + AB_{\mathcal{B}\mathcal{A}}$	$\bullet + \bullet$	-2	+1	-1

that is, resultants from deducting recombinations in Tables 2 and 3 are sources of other deducting recombinations, as shown in Fig. 6. These observations allow the identification of groups of chained recombinations, as listed in Table 4.

Each group is represented by a combinations of letters, where:

- \mathbb{W} represents an $AA_{\mathcal{A}\mathcal{B}}$, $\bar{\mathbb{W}}$ represents an $AA_{\mathcal{A}}$ and $\underline{\mathbb{W}}$ represents an $AA_{\mathcal{B}}$;
- \mathbb{M} represents a $BB_{\mathcal{A}\mathcal{B}}$, $\bar{\mathbb{M}}$ represents a $BB_{\mathcal{A}}$ and $\underline{\mathbb{M}}$ represents a $BB_{\mathcal{B}}$;
- \mathbb{Z} represents an $AB_{\mathcal{A}\mathcal{B}}$ and \mathbb{N} represents an $AB_{\mathcal{B}\mathcal{A}}$.

Although some groups have reusable resultants, those are actually never reused (if groups that are lower in the table use as sources resultants from higher groups, the sources of all referred groups would be previously consumed in groups that occupy even higher positions in the table). Due to this fact, the number of occurrences in each group depends only on the initial number of each type of component.

The deductions shown in Table 4 can be computed with an approach that greedily maximizes the groups in \mathcal{P} , \mathcal{Q} , \mathcal{T} , \mathcal{S} , \mathcal{M} and \mathcal{N} in this order. The \mathcal{P} part contains only one operation and is thus very simple. The same happens with \mathcal{Q} , since the two groups in this part are exclusive after applying \mathcal{P} . The four subparts of \mathcal{T} are also exclusive after applying \mathcal{Q} . (Note that groups $\mathbb{W}\bar{\mathbb{W}}\bar{\mathbb{M}}$, $\mathbb{W}\bar{\mathbb{W}}\underline{\mathbb{M}}$, $\mathbb{M}\bar{\mathbb{M}}\bar{\mathbb{W}}$ and $\mathbb{M}\bar{\mathbb{M}}\underline{\mathbb{W}}$ of \mathcal{T} are simply subgroups of \mathcal{Q} .) The groups in \mathcal{S} correspond to the simple application of all possible remaining operations with $\Delta d = -1$. After applying operations of type $\mathbb{Z}\mathbb{N}$, $\bar{\mathbb{W}}\bar{\mathbb{M}}$ and $\underline{\mathbb{W}}\underline{\mathbb{M}}$, the remaining operations in \mathcal{S} are all exclusive. After \mathcal{S} , the two groups in \mathcal{M} are exclusive and then the same happens to the six groups in \mathcal{N} (that are simply subgroups of \mathcal{M}).

We can now rewrite the theorem that gives the exact formula for the DCJ-indel distance:

Table 3. Path recombinations with $\Delta d = 0$ creating resultants that can be used in recombinations with $\Delta d \leq -1$.

sources	resultants	$\Delta \lambda$	$\ \rho\ $	Δd
$AA_{\mathcal{A}} + AB_{\mathcal{B}\mathcal{A}}$	$\bullet + AA_{\mathcal{A}\mathcal{B}}$	-1	+1	0
$AA_{\mathcal{B}} + AB_{\mathcal{A}\mathcal{B}}$	$\bullet + AA_{\mathcal{A}\mathcal{B}}$	-1	+1	0
$BB_{\mathcal{A}} + AB_{\mathcal{A}\mathcal{B}}$	$\bullet + BB_{\mathcal{A}\mathcal{B}}$	-1	+1	0
$BB_{\mathcal{B}} + AB_{\mathcal{B}\mathcal{A}}$	$\bullet + BB_{\mathcal{A}\mathcal{B}}$	-1	+1	0

sources	resultants	$\Delta \lambda$	$\ \rho\ $	Δd
$AA_{\mathcal{A}} + BB_{\mathcal{B}}$	$\bullet + AB_{\mathcal{A}\mathcal{B}}$	0	0	0
$AA_{\mathcal{B}} + BB_{\mathcal{A}}$	$\bullet + AB_{\mathcal{B}\mathcal{A}}$	0	0	0
$AB_{\mathcal{A}\mathcal{B}} + AB_{\mathcal{A}\mathcal{B}}$	$AA_{\mathcal{A}} + BB_{\mathcal{B}}$	-2	+2	0
$AB_{\mathcal{B}\mathcal{A}} + AB_{\mathcal{B}\mathcal{A}}$	$AA_{\mathcal{B}} + BB_{\mathcal{A}}$	-2	+2	0

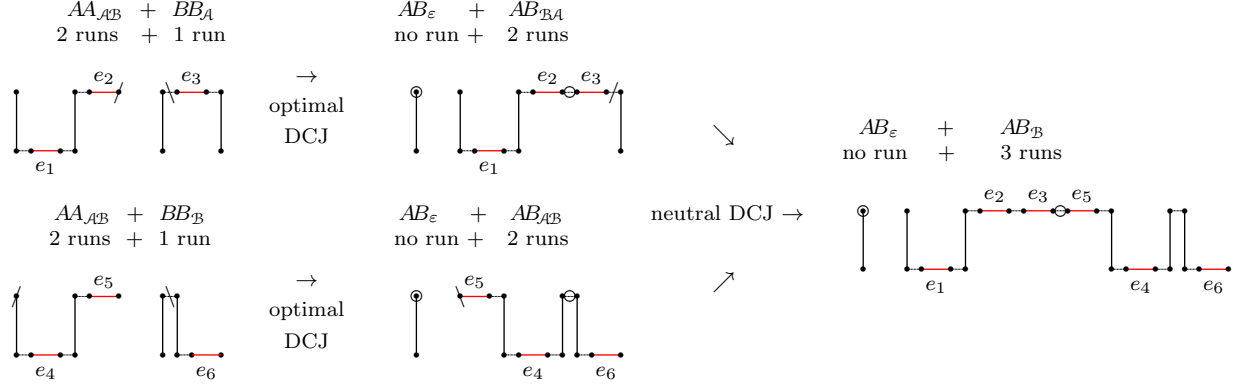


Fig. 6. Chained recombinations transforming four paths ($2 \times AA_{AB} + BB_A + BB_B$) into four other paths ($3 \times AB_\epsilon + AB_B$) with overall $\Delta d = -3$.

Theorem 1 (from [5]). *Given two singular linear genomes A and B , whose relational diagram $R(A, B)$ has c cycles and i AB -paths, we have*

$$d_{DCJ}^{id}(A, B) = |\mathcal{G}| - c - \frac{i}{2} + \sum_{C \in R(A, B)} \lambda(C) - 2\mathcal{P} - 3\mathcal{Q} - 2\mathcal{T} - \mathcal{S} - 2\mathcal{M} - \mathcal{N},$$

where \mathcal{P} , \mathcal{Q} , \mathcal{T} , \mathcal{S} , \mathcal{M} and \mathcal{N} here refer to the number of deductions in the corresponding chained recombination groups.

Table 4. Chained recombination groups obtained from Tables 2 and 3. The column **scr** indicates the contribution of each path in the distance decrease (the table is sorted in descending order with respect to this column).

id	sources			resultants			Δd	scr	
\mathcal{P} \overline{WM}	$AA_{\mathcal{A}\mathcal{B}}$	$BB_{\mathcal{A}\mathcal{B}}$	—	—	—	$2 \times \bullet$	-2	-1	
\mathcal{Q} \overline{WWM}	$2 \times AA_{\mathcal{A}\mathcal{B}}$	$BB_{\mathcal{A}} + BB_{\mathcal{B}}$	—	—	—	$4 \times \bullet$	-3	-3/4	
\overline{MMW}	$AA_{\mathcal{A}} + AA_{\mathcal{B}}$	$2 \times BB_{\mathcal{A}\mathcal{B}}$	—	—	—	$4 \times \bullet$	-3	-3/4	
\mathcal{T} \overline{WZM}	$AA_{\mathcal{A}\mathcal{B}}$	$BB_{\mathcal{A}}$	$AB_{\mathcal{A}\mathcal{B}}$	—	—	$3 \times \bullet$	-2	-2/3	
\overline{WM}	$2 \times AA_{\mathcal{A}\mathcal{B}}$	$BB_{\mathcal{A}}$	—	$AA_{\mathcal{B}}$	—	$2 \times \bullet$	-2	-2/3	
\overline{WNM}	$AA_{\mathcal{A}\mathcal{B}}$	$BB_{\mathcal{B}}$	$AB_{\mathcal{B}\mathcal{A}}$	—	—	$3 \times \bullet$	-2	-2/3	
\overline{WWM}	$2 \times AA_{\mathcal{A}\mathcal{B}}$	$BB_{\mathcal{B}}$	—	$AA_{\mathcal{A}}$	—	$2 \times \bullet$	-2	-2/3	
\overline{MNW}	$AA_{\mathcal{A}}$	$BB_{\mathcal{A}\mathcal{B}}$	$AB_{\mathcal{B}\mathcal{A}}$	—	—	$3 \times \bullet$	-2	-2/3	
\overline{MMW}	$AA_{\mathcal{A}}$	$2 \times BB_{\mathcal{A}\mathcal{B}}$	—	—	$BB_{\mathcal{B}}$	$2 \times \bullet$	-2	-2/3	
\overline{MZW}	$AA_{\mathcal{B}}$	$BB_{\mathcal{A}\mathcal{B}}$	$AB_{\mathcal{A}\mathcal{B}}$	—	—	$3 \times \bullet$	-2	-2/3	
\overline{MMW}	$AA_{\mathcal{B}}$	$2 \times BB_{\mathcal{A}\mathcal{B}}$	—	—	$BB_{\mathcal{A}}$	$2 \times \bullet$	-2	-2/3	
\mathcal{S} \overline{ZN}	—	—	$AB_{\mathcal{A}\mathcal{B}} + AB_{\mathcal{B}\mathcal{A}}$	—	—	$2 \times \bullet$	-1	-1/2	
\overline{WM}	$AA_{\mathcal{A}}$	$BB_{\mathcal{A}}$	—	—	—	$2 \times \bullet$	-1	-1/2	
\overline{WM}	$AA_{\mathcal{B}}$	$BB_{\mathcal{B}}$	—	—	—	$2 \times \bullet$	-1	-1/2	
\overline{WM}	$AA_{\mathcal{A}\mathcal{B}}$	$BB_{\mathcal{A}}$	—	—	$AB_{\mathcal{B}\mathcal{A}}$	\bullet	-1	-1/2	
\overline{WM}	$AA_{\mathcal{A}\mathcal{B}}$	$BB_{\mathcal{B}}$	—	—	$AB_{\mathcal{A}\mathcal{B}}$	\bullet	-1	-1/2	
\overline{WZ}	$AA_{\mathcal{A}\mathcal{B}}$	—	$AB_{\mathcal{A}\mathcal{B}}$	$AA_{\mathcal{A}}$	—	\bullet	-1	-1/2	
\overline{WN}	$AA_{\mathcal{A}\mathcal{B}}$	—	$AB_{\mathcal{B}\mathcal{A}}$	$AA_{\mathcal{B}}$	—	\bullet	-1	-1/2	
\overline{WW}	$2 \times AA_{\mathcal{A}\mathcal{B}}$	—	—	$AA_{\mathcal{B}} + AA_{\mathcal{A}}$	—	—	-1	-1/2	
\overline{MW}	$AA_{\mathcal{A}}$	$BB_{\mathcal{A}\mathcal{B}}$	—	—	$AB_{\mathcal{A}\mathcal{B}}$	\bullet	-1	-1/2	
\overline{MW}	$AA_{\mathcal{B}}$	$BB_{\mathcal{A}\mathcal{B}}$	—	—	$AB_{\mathcal{B}\mathcal{A}}$	\bullet	-1	-1/2	
\overline{MZ}	—	$BB_{\mathcal{A}\mathcal{B}}$	$AB_{\mathcal{A}\mathcal{B}}$	—	$BB_{\mathcal{B}}$	\bullet	-1	-1/2	
\overline{MN}	—	$BB_{\mathcal{A}\mathcal{B}}$	$AB_{\mathcal{B}\mathcal{A}}$	—	$BB_{\mathcal{A}}$	\bullet	-1	-1/2	
\overline{MM}	—	$2 \times BB_{\mathcal{A}\mathcal{B}}$	—	—	$BB_{\mathcal{B}} + BB_{\mathcal{A}}$	—	-1	-1/2	
\mathcal{M} \overline{ZZWM}	$AA_{\mathcal{B}}$	$BB_{\mathcal{A}}$	$2 \times AB_{\mathcal{A}\mathcal{B}}$	—	—	$4 \times \bullet$	-2	-1/2	
\overline{NNWM}	$AA_{\mathcal{A}}$	$BB_{\mathcal{B}}$	$2 \times AB_{\mathcal{B}\mathcal{A}}$	—	—	$4 \times \bullet$	-2	-1/2	
\mathcal{N} \overline{ZW}	$AA_{\mathcal{B}}$	$BB_{\mathcal{A}}$	$AB_{\mathcal{A}\mathcal{B}}$	—	—	$AB_{\mathcal{B}\mathcal{A}}$	$2 \times \bullet$	-1	-1/3
\overline{ZZW}	$AA_{\mathcal{B}}$	—	$2 \times AB_{\mathcal{A}\mathcal{B}}$	$AA_{\mathcal{A}}$	—	—	$2 \times \bullet$	-1	-1/3
\overline{ZZM}	—	$BB_{\mathcal{A}}$	$2 \times AB_{\mathcal{A}\mathcal{B}}$	—	$BB_{\mathcal{B}}$	—	$2 \times \bullet$	-1	-1/3
\overline{NWM}	$AA_{\mathcal{A}}$	$BB_{\mathcal{B}}$	$AB_{\mathcal{B}\mathcal{A}}$	—	—	$AB_{\mathcal{A}\mathcal{B}}$	$2 \times \bullet$	-1	-1/3
\overline{NNW}	$AA_{\mathcal{A}}$	—	$2 \times AB_{\mathcal{B}\mathcal{A}}$	$AA_{\mathcal{B}}$	—	—	$2 \times \bullet$	-1	-1/3
\overline{NNM}	—	$BB_{\mathcal{B}}$	$2 \times AB_{\mathcal{B}\mathcal{A}}$	—	$BB_{\mathcal{A}}$	—	$2 \times \bullet$	-1	-1/3

B Capping of singular genomes and proof of Theorem 3

Before showing how to get an optimal capping of singular genomes with exclusive markers, we will recall a known procedure of capping singular genomes without exclusive markers.

B.1 Capping of canonical genomes

When two singular genomes A and B have no exclusive markers, they are called *canonical genomes*.

The graph $R(A, B)$ of canonical genomes A and B has no indel edges and the indel-potential of any component C is $\lambda(C) = 0$. In this case, the upper bound given by Lemma 1 is tight, and the distance formula can be simplified to $d_{DCJ}^{id}(A, B) = |\mathcal{G}| - c - \frac{i}{2}$, as it was already shown in [2].

Also, obtaining an optimal capping of canonical genomes is quite straightforward [4, 11, 20], as shown in Table 5: the caps should guarantee that each AB -path is closed into a separate cycle, and each pair composed of an AA - and a BB -path is closed into a cycle by linking each extremity of the AA -path to one of the two extremities of the BB -path (there are two possibilities of linking, and any of the two is optimal). If the numbers of linear chromosomes in A and in B are different, there will be some AA - or BB -paths remaining. For each of these an *artificial* adjacency between caps is created in the genome with less linear chromosomes, and each artificial adjacency closes each remaining AA - or BB -path into a separate cycle.

Table 5. Linking paths from $R(A, B)$ of canonical genomes. The symbol Γ_A represents an artificial adjacency in A and the symbol Γ_B represents an artificial adjacency in B . The value Δd corresponds to $\Delta n - \Delta c - \Delta(2i)$.

paths	linking cycle	Δn	Δc	$\Delta(2i)$	Δd
AB	(AB)	+0.5	+1	-0.5	0
$AA + BB$	(AA, BB)	+1	+1	0	0

remaining paths	linking cycle	Δn	Δc	$\Delta(2i)$	Δd
AA	(AA, Γ_B)	+1	+1	0	0
BB	(BB, Γ_A)	+1	+1	0	0

Let κ_A be the total number of linear chromosomes in A and κ_B be the total number of linear chromosomes in B . The difference between the number of AA - or BB -paths is equal to the difference between κ_A and κ_B . In other words, if $R(A, B)$ has a AA -paths, b BB -paths and i AB -paths, the number of artificial adjacencies in such an optimal capping is exactly $a_* = |\kappa_A - \kappa_B| = |a - b|$. Moreover, the number of caps to be added is

$$p_* = \max\{\kappa_A, \kappa_B\} = \max\{a, b\} + \frac{i}{2}.$$

We can show that the capping described above is optimal by verifying the corresponding DCJ-indel distances. Let the original genomes A and B have n markers and $R(A, B)$ have c cycles, besides the paths. Then, after capping, the circular genomes A_o and B_o have $n' = n + p_*$ markers and $R(A_o, B_o)$ has $c' = c + i + \max\{a, b\}$ cycles and no path, so that

$$d_{DCJ}^{id}(A_o, B_o) = n' - c' = n + \max\{a, b\} + \frac{i}{2} - c - i - \max\{a, b\} = n - c - \frac{i}{2} = d_{DCJ}^{id}(A, B).$$

An example of an optimal capping of two canonical linear genomes is given in Fig. 7.

B.2 Singular genomes: correspondence between recombinations and capping

The contents of this part depend on results from [5] presented in Appendix A.

When exclusive markers occur, we can obtain an optimal capping by simply finding caps that properly link the sources of each recombination group (listed in Table 4 of Appendix A) into a single cycle. Indeed, in Table 6 we give a linking that achieves the optimal Δd for each recombination group, followed by the optimal linking of remaining paths. The remaining paths are treated exactly

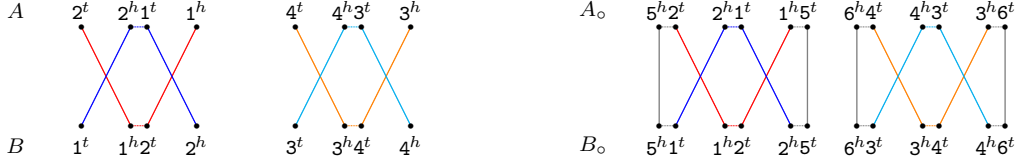


Fig. 7. Optimal capping of canonical genomes $A = \{21, 43\}$ and $B = \{12, 34\}$ into $A_o = \{(215), (436)\}$ and $B_o = \{(125), (346)\}$. Each pair of AA - + BB -path is linked into a separate cycle.

as the linking of paths in canonical genomes. By greedily linking the paths following a top-down order of the referred Table 6 we clearly obtain an optimal capping that transforms A and B into circular genomes A_o and B_o with $d_{DCJ}^{id}(A_o, B_o) = d_{DCJ}^{id}(A, B)$. See an example in Fig. 8.

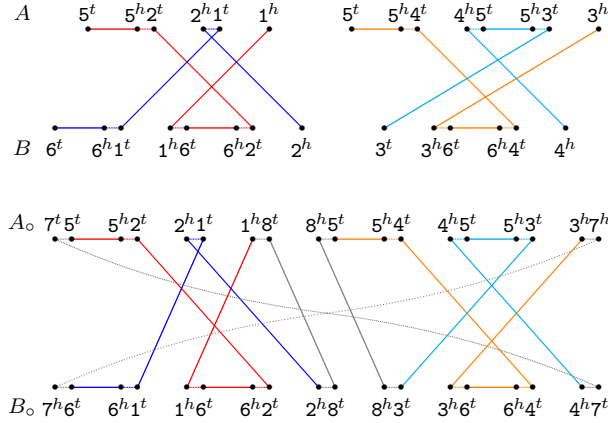


Fig. 8. Optimal capping of singular genomes $A = \{521, 5453\}$ and $B = \{6162, 364\}$ into $A_o = \{(\overline{752185453})\}$ and $B_o = \{(\overline{761628364})\}$. This capping shows how to optimally link the four sources of the chained recombinations of Fig. 6 (Appendix A) into a single cycle.

Furthermore, similarly to the case of canonical genomes, the numbers of artificial adjacencies and caps in such capping are respectively $a_* = |\kappa_A - \kappa_B|$ and $p_* = \max\{\kappa_A, \kappa_B\}$ as we will show in the following.

In Table 6 we can observe that there are two types of groups: (i) balanced, that contain the same number of AA - and BB -paths, and (ii) unbalanced, in which the numbers of AA - and BB -paths are distinct. Unbalanced groups require some extra elements to link the cycle. These elements can be indel-free AA - or BB -paths (of the type that is under-represented in the group) or, if these paths do not exist, artificial adjacencies either in genome A or in genome B (again, of the genome that is under-represented in the group). We then need to examine these unbalanced groups to determine the number of caps and of artificial adjacencies that are required for an optimal capping.

Proposition 2. *If an unbalanced group over-represented in genome A (respectively in genome B) is being linked, there cannot be any remaining indel-enclosing BB -path (respectively AA -path).*

Proof. Without loss of generality, suppose an unbalanced group over-represented in genome A is being linked. If, at this point, there is a remaining indel-enclosing BB -path, with the components of the group being linked and the existing remaining path we would form a balanced group that appears in a higher position of the table, with at least the same Δd , which is a contradiction. \square

As a consequence of Proposition 2, when an unbalanced group is being linked, either there are only indel-free AA - or BB -paths (of the genome that is under-represented) and one of those can be

used to link the group, or there is no AA - or BB -path (of the genome that is under-represented) and an artificial adjacency links the group.

Proposition 3. *In an optimal capping either we have only unbalanced groups that are over-represented in genome A or we have only unbalanced groups that are over-represented in genome B .*

Proof. It is clear that, after \mathcal{P} and until \mathcal{N} , we either have only groups W^* (over-represented in A), or only groups M^* (over-represented in B). The question is whether groups in \mathcal{N} that are over-represented in B are compatible with previous groups of type W^* and, symmetrically, whether groups in \mathcal{N} that are over-represented in A are compatible with previous groups of type M^* .

Let us examine the case of group $ZZ\underline{W}$. (i) At a first glance one could think that this group is compatible with $MM\underline{W}$. However, if all components of these two unbalanced groups would be in the graph, we would instead have two times the group $MZ\underline{W}$, that is balanced and located before the two other groups in the table (observe that $2 \times MZ\underline{W}$ has a smaller Δd than $ZZ\underline{W} + MM\underline{W}$). (ii) When we test the compatibility of $ZZ\underline{W}$ with $MM\underline{W}$, we see that with the same components we would get $MM\underline{W}$, that is balanced and located before the two other groups in the table (observe that $MM\underline{W}$ has the same Δd as $ZZ\underline{W} + MM\underline{W}$).

With a similar analysis we can show that for all cases either we have only unbalanced groups that are over-represented in genome A or we have only unbalanced groups that are over-represented in genome B . \square

Propositions 2 and 3 prove the following result.

Theorem 3. *Let κ_A and κ_B be, respectively, the total numbers of linear chromosomes in singular genomes A and B . The number of caps in the optimal capping given by Table 6 is*

$$p_* = \max\{\kappa_A, \kappa_B\}$$

and the number of artificial adjacencies between caps is $a_ = |\kappa_A - \kappa_B|$.*

B.3 Figure illustrating a capped multi-relational diagram of natural genomes

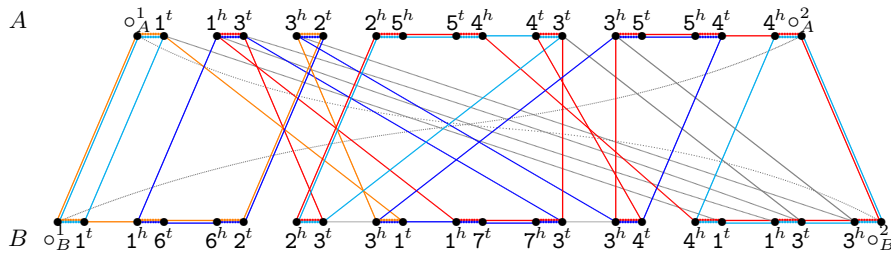


Fig. 9. Natural genomes $A = 1325\bar{4}354$ and $B = 1623173413$ and their capped multi-relational diagram $MR_o(A, B)$

Table 6. Linking sources of chained recombination groups from Table 4 (Appendix A). The symbol Γ_A represents an artificial adjacency in A and the symbol Γ_B represents an artificial adjacency in B . The notation $AA_\varepsilon \prec \Gamma_A$ means that a AA_ε path is preferred to close the cycle, but if it does not exist, we take an artificial adjacency in A . In order to give the correct order of linking, we sometimes need to represent a path $AB_{\mathcal{A}\mathcal{B}}$ by $BA_{\mathcal{B}\mathcal{A}}$ and a path $AB_{\mathcal{B}\mathcal{A}}$ by $BA_{\mathcal{A}\mathcal{B}}$. The value Δd corresponds to $\Delta n - \Delta c - \Delta(2i) + \Delta\lambda$. Unbalanced groups over-represented in genome A are marked with a “ \cup ”, while unbalanced groups over-represented in genome B are marked with a “ \cap ”.

id	sources	linking cycle	T	Δn	Δc	$\Delta(2i)$	$\Delta\lambda$	Δd
\mathcal{P} \underline{WM}	$AA_{\mathcal{A}\mathcal{B}} + BB_{\mathcal{A}\mathcal{B}}$	$(AA_{\mathcal{A}\mathcal{B}}, BB_{\mathcal{B}\mathcal{A}})$		+1	+1	0	-2	-2
\mathcal{Q} \underline{WWM}	$2 \times AA_{\mathcal{A}\mathcal{B}} + BB_{\mathcal{A}} + BB_{\mathcal{B}}$	$(AA_{\mathcal{A}\mathcal{B}}, BB_{\mathcal{B}}, AA_{\mathcal{B}\mathcal{A}}, BB_{\mathcal{A}})$		+2	+1	0	-4	-3
\underline{MMW}	$2 \times BB_{\mathcal{A}\mathcal{B}} + AA_{\mathcal{A}} + AA_{\mathcal{B}}$	$(BB_{\mathcal{A}\mathcal{B}}, AA_{\mathcal{B}}, BB_{\mathcal{B}\mathcal{A}}, AA_{\mathcal{A}})$		+2	+1	0	-4	-3
\mathcal{T} \underline{WZM}	$AA_{\mathcal{A}\mathcal{B}} + BB_{\mathcal{A}} + AB_{\mathcal{A}\mathcal{B}}$	$(AB_{\mathcal{A}\mathcal{B}}, AA_{\mathcal{B}\mathcal{A}}, BB_{\mathcal{A}})$		+1.5	+1	-0.5	-3	-2
\underline{WWM}	$2 \times AA_{\mathcal{A}\mathcal{B}} + BB_{\mathcal{A}}$	$(AA_{\mathcal{B}\mathcal{A}}, BB_{\mathcal{A}}, AA_{\mathcal{A}\mathcal{B}}, BB_\varepsilon \prec \Gamma_B)$	\cup	+2	+1	0	-3	-2
\underline{WNM}	$AA_{\mathcal{A}\mathcal{B}} + BB_{\mathcal{B}} + AB_{\mathcal{B}\mathcal{A}}$	$(AB_{\mathcal{B}\mathcal{A}}, AA_{\mathcal{A}\mathcal{B}}, BB_{\mathcal{B}})$		+1.5	+1	-0.5	-3	-2
\underline{WWM}	$2 \times AA_{\mathcal{A}\mathcal{B}} + BB_{\mathcal{B}}$	$(AA_{\mathcal{A}\mathcal{B}}, BB_{\mathcal{A}}, AA_{\mathcal{A}\mathcal{B}}, BB_\varepsilon \prec \Gamma_B)$	\cup	+2	+1	0	-3	-2
\underline{MNW}	$BB_{\mathcal{A}\mathcal{B}} + AA_{\mathcal{A}} + AB_{\mathcal{B}\mathcal{A}}$	$(AB_{\mathcal{B}\mathcal{A}}, AA_{\mathcal{A}}, BB_{\mathcal{A}\mathcal{B}})$		+1.5	+1	-0.5	-3	-2
\underline{MMW}	$2 \times BB_{\mathcal{A}\mathcal{B}} + AA_{\mathcal{A}}$	$(BB_{\mathcal{B}\mathcal{A}}, AA_{\mathcal{A}}, BB_{\mathcal{A}\mathcal{B}}, AA_\varepsilon \prec \Gamma_A)$	\cap	+2	+1	0	-3	-2
\underline{MZW}	$BB_{\mathcal{A}\mathcal{B}} + AA_{\mathcal{B}} + AB_{\mathcal{A}\mathcal{B}}$	$(AB_{\mathcal{A}\mathcal{B}}, AA_{\mathcal{B}}, BB_{\mathcal{B}\mathcal{A}})$		+1.5	+1	-0.5	-3	-2
\underline{MMW}	$2 \times BB_{\mathcal{A}\mathcal{B}} + AA_{\mathcal{B}}$	$(BB_{\mathcal{A}\mathcal{B}}, AA_{\mathcal{B}}, BB_{\mathcal{B}\mathcal{A}}, AA_\varepsilon \prec \Gamma_A)$	\cap	+2	+1	0	-3	-2
\mathcal{S} \underline{ZN}	$AB_{\mathcal{A}\mathcal{B}} + AB_{\mathcal{B}\mathcal{A}}$	$(AB_{\mathcal{A}\mathcal{B}}, AB_{\mathcal{B}\mathcal{A}})$		+1	+1	-1	-2	-1
\underline{WM}	$AA_{\mathcal{A}} + BB_{\mathcal{A}}$	$(AA_{\mathcal{A}}, BB_{\mathcal{A}})$		+1	+1	0	-1	-1
\underline{WM}	$AA_{\mathcal{B}} + BB_{\mathcal{B}}$	$(AA_{\mathcal{B}}, BB_{\mathcal{B}})$		+1	+1	0	-1	-1
\underline{WM}	$AA_{\mathcal{A}\mathcal{B}} + BB_{\mathcal{A}}$	$(AA_{\mathcal{B}\mathcal{A}}, BB_{\mathcal{A}})$		+1	+1	0	-1	-1
\underline{WM}	$AA_{\mathcal{A}\mathcal{B}} + BB_{\mathcal{B}}$	$(AA_{\mathcal{A}\mathcal{B}}, BB_{\mathcal{B}})$		+1	+1	0	-1	-1
\underline{WZ}	$AA_{\mathcal{A}\mathcal{B}} + AB_{\mathcal{A}\mathcal{B}}$	$(AA_{\mathcal{B}\mathcal{A}}, BB_\varepsilon \prec \Gamma_B, AB_{\mathcal{A}\mathcal{B}})$	\cup	+1.5	+1	-0.5	-2	-1
\underline{WN}	$AA_{\mathcal{A}\mathcal{B}} + AB_{\mathcal{B}\mathcal{A}}$	$(AA_{\mathcal{A}\mathcal{B}}, BB_\varepsilon \prec \Gamma_B, AB_{\mathcal{B}\mathcal{A}})$	\cup	+1.5	+1	-0.5	-2	-1
\underline{WW}	$AA_{\mathcal{A}\mathcal{B}} + AA_{\mathcal{A}\mathcal{B}}$	$(AA_{\mathcal{A}\mathcal{B}}, BB_\varepsilon \prec \Gamma_B, AA_{\mathcal{B}\mathcal{A}}, BB_\varepsilon \prec \Gamma_B)$	\cup	+2	+1	0	-2	-1
\underline{MW}	$BB_{\mathcal{A}\mathcal{B}} + AA_{\mathcal{A}}$	$(AA_{\mathcal{A}}, BB_{\mathcal{A}\mathcal{B}})$		+1	+1	0	-1	-1
\underline{MW}	$BB_{\mathcal{A}\mathcal{B}} + AA_{\mathcal{B}}$	$(AA_{\mathcal{B}}, BB_{\mathcal{B}\mathcal{A}})$		+1	+1	0	-1	-1
\underline{MZ}	$BB_{\mathcal{A}\mathcal{B}} + AB_{\mathcal{A}\mathcal{B}}$	$(BB_{\mathcal{B}\mathcal{A}}, AB_{\mathcal{A}\mathcal{B}}, AA_\varepsilon \prec \Gamma_A)$	\cap	+1.5	+1	-0.5	-2	-1
\underline{MN}	$BB_{\mathcal{A}\mathcal{B}} + AB_{\mathcal{B}\mathcal{A}}$	$(BB_{\mathcal{A}\mathcal{B}}, AB_{\mathcal{B}\mathcal{A}}, AA_\varepsilon \prec \Gamma_A)$	\cap	+1.5	+1	-0.5	-2	-1
\underline{MM}	$BB_{\mathcal{A}\mathcal{B}} + BB_{\mathcal{A}\mathcal{B}}$	$(BB_{\mathcal{A}\mathcal{B}}, AA_\varepsilon \prec \Gamma_A, BB_{\mathcal{B}\mathcal{A}}, AA_\varepsilon \prec \Gamma_A)$	\cap	+2	+1	0	-2	-1
\mathcal{M} \underline{ZZWM}	$2 \times AB_{\mathcal{A}\mathcal{B}} + AA_{\mathcal{B}} + BB_{\mathcal{A}}$	$(AB_{\mathcal{A}\mathcal{B}}, AA_{\mathcal{B}}, BA_{\mathcal{B}\mathcal{A}}, BB_{\mathcal{A}})$		+2	+1	-1	-4	-2
\underline{NNWM}	$2 \times AB_{\mathcal{B}\mathcal{A}} + AA_{\mathcal{A}} + BB_{\mathcal{B}}$	$(AB_{\mathcal{B}\mathcal{A}}, AA_{\mathcal{A}}, BA_{\mathcal{A}\mathcal{B}}, BB_{\mathcal{B}})$		+2	+1	-1	-4	-2
\mathcal{N} \underline{ZWM}	$AB_{\mathcal{A}\mathcal{B}} + AA_{\mathcal{B}} + BB_{\mathcal{A}}$	$(AB_{\mathcal{A}\mathcal{B}}, AA_{\mathcal{B}}, BB_{\mathcal{A}})$		+1.5	+1	-0.5	-2	-1
\underline{ZZW}	$2 \times AB_{\mathcal{A}\mathcal{B}} + AA_{\mathcal{B}}$	$(AB_{\mathcal{A}\mathcal{B}}, AA_{\mathcal{B}}, BA_{\mathcal{B}\mathcal{A}}, BB_\varepsilon \prec \Gamma_B)$	\cup	+2	+1	-1	-3	-1
\underline{ZZM}	$2 \times AB_{\mathcal{A}\mathcal{B}} + BB_{\mathcal{A}}$	$(BA_{\mathcal{B}\mathcal{A}}, BB_{\mathcal{A}}, AB_{\mathcal{A}\mathcal{B}}, AA_\varepsilon \prec \Gamma_A)$	\cap	+2	+1	-1	-3	-1
\underline{NWM}	$AB_{\mathcal{B}\mathcal{A}} + AA_{\mathcal{A}} + BB_{\mathcal{B}}$	$(AB_{\mathcal{B}\mathcal{A}}, AA_{\mathcal{A}}, BB_{\mathcal{B}})$		+1.5	+1	-0.5	-2	-1
\underline{NNW}	$2 \times AB_{\mathcal{B}\mathcal{A}} + AA_{\mathcal{A}}$	$(AB_{\mathcal{B}\mathcal{A}}, AA_{\mathcal{A}}, BA_{\mathcal{A}\mathcal{B}}, BB_\varepsilon \prec \Gamma_B)$	\cup	+2	+1	-1	-3	-1
\underline{NNM}	$2 \times AB_{\mathcal{B}\mathcal{A}} + BB_{\mathcal{B}}$	$(BA_{\mathcal{A}\mathcal{B}}, BB_{\mathcal{B}}, AB_{\mathcal{B}\mathcal{A}}, AA_\varepsilon \prec \Gamma_A)$	\cap	+2	+1	-1	-3	-1
	remaining paths	linking cycle		Δn	Δc	$\Delta(2i)$	$\Delta\lambda$	Δd
	AB_*	(AB_*)		+0.5	+1	-0.5	0	0
	$AA_* + BB_*$	(AA_*, BB_*)		+1	+1	0	0	0
	AA_*	(AA_*, Γ_B)	\cup	+1	+1	0	0	0
	BB_*	(BB_*, Γ_A)	\cap	+1	+1	0	0	0

C Performance benchmark details

In the following, we describe our simulation tool that has been used for the analysis presented in Section 4.2. The software is included in our software repository (<https://gitlab.ub.uni-bielefeld.de/gi/ding>).

Our method samples marker order sequences over a user-defined phylogeny. However, our simulations are restricted to pairwise comparisons generated over rooted, weighted trees of two leaves. Starting from an initial marker order sequence of user-defined length (i.e., number of markers), the simulator samples Poisson-distributed DCJ events with expectation equal to the corresponding edge weights. Likewise, insertion, deletion and duplication events of one or more consecutive markers are sampled, yet, their frequency is additionally dependent on a *rate factor* that can be adjusted by the user. The length of each segmental insertion, deletion, and duplication is drawn from a Zipf distribution, whose parameters can also be adjusted by the user. At each internal node of the phylogeny, the succession of mutational operations is performed in the following order: DCJ operations, duplications, deletions, insertions. To this end, cut points, as well as locations for insertions, deletions and duplications are uniformly drawn over the entire genome.

In our simulations, we used $s = 4$ for zipfian distributions of insertions and deletions, and $s = 6$ for duplications. Unless specified otherwise, insertion and deletion rates were set to be 0.1 and 0.2 respectively. We set the length of the root genome to 20,000 markers.

D Analysis of high-resolution human genome data

Recently, the first three high-resolution haplotype-resolved human genomes have been published, representing a Han Chinese (HG00514), a Puerto Rican (HG00733), and a Yoruban Nigerian (NA19240) individual, respectively [8]. Each of these individuals contribute two sets of 23 chromosomes that we call genomes h0 and h1, respectively. The analysis in this work is confined to the comparison of the HG00514.h0 genome with the human reference sequence (GRCh38).

Construction of Genomic marker set. The computation of the here proposed rearrangement measure depends on pre-defined genomic markers. To obtain such markers from the studied human genome data set, we used GEESE [15]. GEESE implements a heuristic for the genome segmentation problem [19] and takes as input local pairwise sequence alignments. These were computed by LASTZ with parameter settings “--step=10 --gapped --gfextend --ambiguous=iupac --masking=5 --filter=identity:95 --hspthresh=90000”. Furthermore, we used the following scoring scheme which has been inferred from the genomic data set:

```
bad_score      = X:-1323 # used for sub[X][*] and sub[*][X]
fill_score     = -132    # used when sub[*][*] not otherwise defined
gap_open_penalty = 430
gap_extend_penalty = 32
```

	A	C	G	T
A	90	-120	-81	-119
C	-120	100	-132	-81
G	-81	-132	100	-120
T	-119	-81	-120	90

Table 7. Overview of high-resolution human genome dataset. Columns from left to right: Chromosome number, number of markers in each of the twenty-three chromosomes of both genomes, agreement of marker set of the reference genome with SV call set of Chaisson *et al.* [8], running time of the ILP for the pairwise comparison (“-” indicates that no exact solution was found—instead, the optimality gap is specified in brackets), the DCJ-indel distance of the computed solution, and the reported number of runs.

chr.	HG00514.h0	GRCh38	SV agreement	solving time[s]	distance	#runs
1	17930	17687	78.79%	- (0.14%)	720	376
2	16897	16714	74.80%	-(0.09%)	653	361
3	13725	13484	81.18%	22.64	446	280
4	13587	13612	78.12%	9.73	557	313
5	13188	12958	76.47%	- (0.05%)	488	285
6	12698	12502	69.09%	24.95	615	327
7	13393	13331	74.17%	187.48	615	315
8	10626	10357	75.26%	246.71	434	243
9	10536	10820	75.11%	- (0.20%)	649	287
10	10359	10287	71.10%	29.74	481	283
11	10410	10304	78.03%	135.15	521	273
12	9532	9402	72.69%	3.55	463	269
13	6989	6752	72.88%	4.28	246	192
14	6033	5994	74.65%	2.92	251	139
15	6843	6743	74.27%	- (0.12%)	268	150
16	7283	7142	73.41%	- (0.32%)	384	195
17	7595	7413	67.06%	198.89	363	205
18	5260	5060	75.31%	1.60	225	144
19	6260	6047	66.18%	361.09	359	210
20	4525	4367	66.23%	1.67	271	139
21	2725	3054	66.56%	6.86	332	112
22	3888	3989	69.62%	1952.66	336	149
X	8055	8493	82.67%	17.58	526	247
<i>total</i>	218337	216512	73.63%	/	/	/

We then ran GEESE on the computed alignments to construct genomic markers of length at least 500bp using the following parameter settings: `--minLength 500 --minIdent 90 --maxGap 50 --minAlnLength 20`. An overview of the number of markers obtained for each chromosome is given in Table 7. Figure 10 shows a histogram of the multiplicities of markers in both genomes.

Comparison with structural variation data set. To assess the quality of our marker set, we compare the breakpoints that are introduced by the markers with breakpoints of identified *structural variations* (SVs) in the data set. Chaisson *et al.* [8] unified call sets of structural variations from a range of different technologies into a single call set that is made available at:

ftp://ftp.1000genomes.ebi.ac.uk/vol1/ftp/data_collections/hgsv_sv_discovery/working/20180627_PanTechnologyIntegrationSet

Note that largest fraction (47%) of called SVs is associated with tandem repeats and other repetitive elements, whose exact number and precise location depends heavily on the parameter choices of the employed detection algorithms, as the authors remark in their paper [8]. Structural variations introduce breakpoints in the pairwise alignment of genomic sequences. We assess the quality of our genomic marker set by quantifying the number of markers that are in agreement with these breakpoints, i.e., that are not disrupted by a boundary of an SV from the call set. To this end, we mapped the SV breakpoints to the reference genome and compared them with the marker set of the reference genome. The outcome of this analysis is summarized in the “SV agreement” column of Table 7.

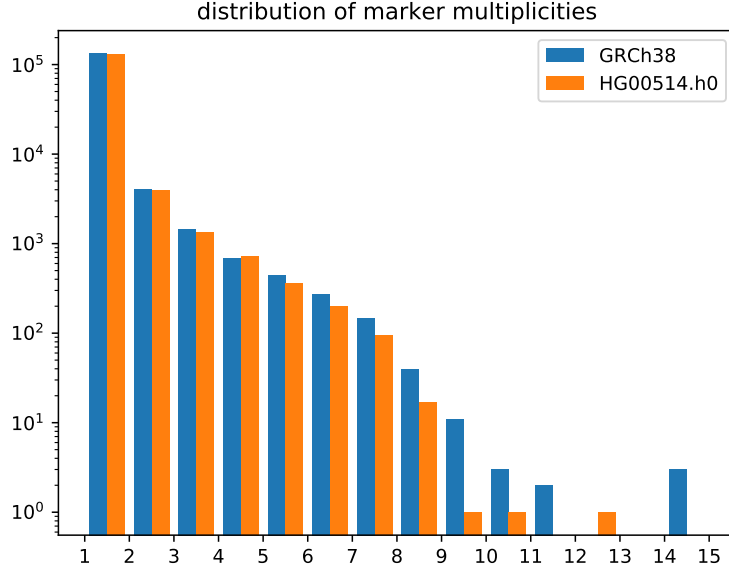


Fig. 10. Number of occurrences (y-axis) for each marker multiplicity (x-axis) in genomes GRCh38 and HG00514.h0.

DCJ-indel distance computation. Using CPLEX v12.6 as solver, we applied the ILP described in Section 4 to each of the twenty-three pairs of chromosomes of HG00514.h0 and GRCh38. Each computation was run on a single thread on a compute cluster populated with different state-of-the-art hardware (e.g., Intel Xeon E7540 processors). We set CPLEX to terminate the search for an optimal solution after at most 12h of running time. The results of these calculations are summarized in the last three columns of Table 7. For chromosomes 1, 2, 5, 15 and 16, no optimal solution was found within the time limit. In those cases, column “solving time[s]” shows in brackets the optimality gap instead. The *optimality gap* is defined as difference in percentage between the best primal and the best dual solution so far identified by the solver.